

Gamma Ray Signal from the Pulsar Wind in the Binary Pulsar system PSR B1259–63/LS 2883

Dmitry Khangulyan¹, Felix A. Aharonian^{2,3} Sergey V. Bogovalov⁴, Marc Ribó⁵

¹*Institute of Space and Astronautical Science/JAXA, 3-1-1 Yoshinodai, Chuo-ku, Sagami-hara, Kanagawa 252-5210, Japan*

khangul@astro.isas.jaxa.jp

²*Dublin Institute for Advanced Studies, 31 Fitzwilliam Place, Dublin 2, Ireland*

felix.aharonian@dias.ie

³*Max-Planck-Institut für Kernphysik, Saupfercheckweg 1, D-69117 Heidelberg, Germany*

⁴*National research nuclear university-MEPHI, Kashirskoe shosse 31, Moscow, 115409 Russia*

svbogovalov@mephi.ru

⁵*Departament d'Astronomia i Meteorologia, Institut de Ciències del Cosmos (ICC), Universitat de Barcelona (IEEC-UB), Martí i Franquès 1, E-08028 Barcelona, Spain*

mribo@am.ub.es

ABSTRACT

Binary pulsar systems emit potentially detectable components of gamma ray emission due to Comptonization of the optical radiation of the companion star by relativistic electrons of the pulsar wind, both before and after termination of the wind. The recent optical observations of binary pulsar system PSR B1259–63/LS 2883 revealed radiation properties of the companion star which differ significantly from previous measurements. In this paper we study the implications of these observations for the interaction rate of the unshocked pulsar wind with the stellar photons and the related consequences for fluxes of high energy (HE) and very high energy (VHE) gamma rays. We show that the signal should be strong enough to be detected with *Fermi* close to the periastron passage, unless the pulsar wind is strongly anisotropic or the Lorentz factor of the wind is smaller than 10^3 or larger than 10^5 . The higher luminosity of the optical star also has two important implications: (i) attenuation of gamma rays

due to photon-photon pair production, and (ii) Compton drag of the unshocked wind. While the first effect has an impact on the lightcurve of VHE gamma rays, the second effect may significantly decrease the energy available for particle acceleration after termination of the wind.

Subject headings: binaries: close — gamma rays: stars — pulsars: individual (PSR B1259–63)

1. Introduction

Three binary systems containing a massive star and a compact object – LS 5039, LS I +61 303 and PSR B1259–63– have been clearly detected in TeV energy band (see <http://tevcat.uchicago.edu/> for the updated information). While the nature of the compact companion in LS 5039 and LS I +61 303 is not yet established (Casares et al. 2005a,b; Sarty et al. 2011), the detection of the pulsed radio emission from PSR B1259–63 indicates the presence of a 47.7 ms pulsar in the system (Johnston et al. 1992). The pulsar orbits a luminous star in a very eccentric orbit with the following orbital parameters: eccentricity $e = 0.87$, period $P_{\text{orb}} = 1237$ d, and semi-major axis $a_2 = 6.9$ AU (see Negueruela et al. 2011, and references therein). The system displays variable broadband nonthermal radio, X-ray and TeV gamma ray emission close to periastron passage (Johnston et al. 2005; Uchiyama et al. 2009; Chernyakova et al. 2009; Grove et al. 1995; Aharonian et al. 2005, 2009), which currently lacks successful multiwavelength interpretations. Moreover, the *Fermi* LAT observations of periastron passage in December 2010 have shown that in general the GeV flux level from the system is quite low, although a short intensive flare was detected as well (see e.g. Tam et al. 2011; Abdo et al. 2011).

Recently, optical observations with VLT UT2 Kueyen discovered that the optical star LS 2883 corresponds to a late O-star and has a significantly higher luminosity of $L_* = 2.3 \times 10^{38}$ erg s⁻¹ than previously thought (Negueruela et al. 2011). Because of fast rotation the star is significantly oblated with equatorial radius of $R_{\text{eq}} = 9.7R_{\odot}$ and the polar radius of $R_{\text{pole}} = 8.1R_{\odot}$. This leads as well to a strong gradient of the star surface temperature with $T_{\text{eq}} = 27\,500$ K and $T_{\text{pole}} = 34\,000$ K. The star rotation axis is inclined by $i_* \simeq 33^\circ$ in respect to the line-of-sight (Negueruela et al. 2011). The distance to the system is now estimated to be 2.3 ± 0.4 kpc. Moreover, the observations favored an orbital inclination value of $i \simeq 25^\circ$, which is remarkably smaller than the previously obtained value of $\sim 35^\circ$ (Johnston et al. 1994). All these new parameters together should have an important impact on the multiwavelength properties of this system.

The orbital separation distance, pulsar spindown luminosity and the lack of the accretion features suggest a realization of the compactified nebula scenario, i.e. the source contains two distinct regions: the relativistic pulsar wind and the terminated flow (Tavani & Arons 1997; Bogovalov et al. 2008). The VHE emission is expected to originate in the post termination shock region, and a number of models have been proposed invoking both hadronic (Kawachi et al. 2004; Neronov & Chernyakova 2007) and leptonic (Kirk et al. 1999; Khangulyan et al. 2007) radiation mechanisms. In the framework of the hadronic scenario, the two humped TeV lightcurve obtained with HESS in 2004 (Aharonian et al. 2005) have been interpreted as the enhancement of the production rate due to the pulsar passage through the dense stellar disc. However, the recent report of a more complicated TeV gamma ray lightcurve by HESS with multiple humps and deeps disfavors, to a large extent, the hadronic scenario (Aharonian et al. 2009). In the case of leptonic origin of the emission, there is a number of additional effects, which may significantly affect the production rate of the nonthermal emission in the post shock region (Khangulyan et al. 2007). Importantly, in the leptonic scenario, one expects a specific radiation component from the unshocked pulsar wind. Although, the pulsar wind region is not expected to produce VHE emission, a line-like bulk Comptonization component from this region in HE band is predicted for isolated pulsars like Crab pulsar (Bogovalov & Aharonian 2000) and for the binary pulsar system PSR B1259–63 (Ball & Kirk 2000; Ball & Dodd 2001; Khangulyan et al. 2007). It is difficult to overestimate the importance of observational proof of this radiation component; it offers a unique opportunity of detecting a direct signal from the pulsar wind. The most meaningful constraints in this regard can be obtained in the 1 to 100 GeV region. Therefore the observations with *Fermi* and *AGILE* gamma ray telescopes close to the periastron passage are of great interest; any result (flux upper limit or detections of a signal) can greatly contribute to our understanding of the physics of pulsar winds.

Since the interaction of the pulsar wind with the stellar photon field does not occur in the *saturation regime*, the production rate is very sensitive to the properties of the photon field. In this paper we present new calculations of the radiation signal from the pulsar wind taking into account the new properties of the optical star (Negueruela et al. 2011) and using results of detailed hydrodynamical modeling of the interaction between the pulsar and stellar winds in PSR B1259–63/LS 2883 (Bogovalov et al. 2008).

2. Pulsar Wind in Binary Pulsar System

In the framework of the generally accepted paradigm (Kennel & Coroniti 1984), pulsars launch cold ultrarelativistic winds which are terminated due to external pressure. At the

termination shock, the wind electrons can be accelerated to multi-TeV energies. The radiation of these electrons results in a phenomenon called pulsar wind nebula. Since the wind is cold, i.e. particles remain at rest in the wind co-moving system, no synchrotron emission is expected from the wind before its termination. On the other hand, the comptonization of the ultrarelativistic wind by external radiation fields, through which the wind propagates, can lead to detectable gamma ray emission. This effect is relatively weak in isolated pulsars, and can achieve a reasonable efficiency only in powerful pulsars, provided that the particle dominated wind is formed close to the light cylinder (Bogovalov & Aharonian 2000). In binary systems, the process operates with an enhanced efficiency thanks to the presence of the dense radiation field of the optical companion (Ball & Kirk 2000; Ball & Dodd 2001). The interaction rate in this channel depends on different parameters characterizing the system: (i) luminosity and temperature of the optical star; (ii) orbital separation and inclination; (iii) distance to the system; (iv) size of the region occupied by the pulsar wind; (v) pulsar wind bulk Lorentz factor.

Remarkably, the recent optical observations of PSR B1259–63 have significantly revised the parameters (i), (ii) and (iii) in favor of higher temperature and luminosity, smaller inclination angle and further system location. Regarding the wind bulk Lorentz factor, it remains a highly uncertain parameter.

The size of the region, where the pulsar wind can propagate depends on the ratio of the wind ram pressures, η (Bogovalov et al. 2008). Since the pulsar spindown luminosity is known, one can estimate the ram pressure of the pulsar wind

$$P_{\text{pw}} = \frac{L_{\text{sd}}}{4\pi r^2 c}, \quad (1)$$

where L_{sd} and r are the spindown luminosity of the pulsar and distance to the pulsar, respectively. It should be noted that this relation ignores the possible effects related to the anisotropy of the pulsar wind. Although, the level of the anisotropy may be quite high at large distances from the pulsar, e.g. in the case of the Crab-like pulsars (Bogovalov & Khangoulyan 2002), in this paper we limit our consideration by the case of an isotropic wind.

To obtain the ram pressure of the stellar wind, one needs detailed information about the properties of the optical star, including the mass-loss rate and wind velocity profile, which are currently not firmly established. For the given optical star luminosity, the mass-loss rate can be estimated at the level of $\dot{M} = 6 \times 10^{-8} M_{\odot} \text{yr}^{-1}$ (Vink et al. 2000). Accounting for the wind velocity at interaction point $V_w < V_{\infty} = 1350 \pm 200 \text{ km s}^{-1}$ (McCollum 1993), it is possible to estimate the expected value of the ratio of the momentum flux densities,

η -parameter, as follows:

$$\eta = \frac{L_{\text{sd}}}{\dot{M}cV_w} = 5 \times 10^{-2} \left(\frac{\dot{M}}{6 \times 10^{-8} M_{\odot} \text{yr}^{-1}} \right)^{-1} \left(\frac{V_w}{1350 \text{ km s}^{-1}} \right)^{-1}. \quad (2)$$

We should note, however, that there are several factors which may introduce significant uncertainties in the η -parameter. In particular, the wind porosity may lead to an overestimation of the mass-loss rate of the star (Owocki & Cohen 2006) and consequently to a significant underestimate of the η parameter value. The opposite situation may occur if the pulsar wind interacts with the stellar wind close to the star equatorial plane, where a dense Keplerian disk is formed. Since the disk is expected to have a significantly higher density than the polar wind, and its typical velocity at distance r (i.e. Keplerian velocity) may be as high as

$$v_{\text{disk}} \simeq 200 \left(\frac{r}{10^{13} \text{ cm}} \right)^{-1/2} \text{ km s}^{-1}, \quad (3)$$

the disk effective ram pressure may significantly exceed the polar wind one, i.e. the η -parameter may be remarkably smaller than the estimate of Eq.(2). Moreover, because of the disk rotation and pulsar orbital velocity, the structure of the wind termination shock, in respect to the observer direction, may be rather different for two pulsar–disk interaction points. Because of these uncertainties related to the value of the η -parameter, below we will consider a fairly broad range of the η parameter.

In Figure 1 the shapes of the termination shock for three different values of the η parameter are shown. The points in the figure are from the results of numerical modeling performed by Bogovalov et al. (2008), for $\eta = 1$ (squares), $\eta = 0.05$ (filled circles) and $\eta = 1.1 \times 10^{-3}$ (open circles). Here the value of $\eta = 1$ roughly corresponds to the case of the interaction with the clumpy polar wind; $\eta = 0.05$ to the case of collision with the stellar wind; and $\eta = 1.1 \times 10^{-3}$ is a lower limit value, which can be realized if e.g. pulsar wind is significantly anisotropic at binary system scales; or if the stellar disk plays an important role in the interaction. To simplify the calculations we have approximated the termination shock by the following analytical expressions:

for $\eta = 1$

$$r = 3.02 \sqrt{(z + 0.425649)(z + 0.92)}, \quad (4)$$

for $\eta = 0.05$

$$r = 0.33 \sqrt{(z + 0.167)(z + 5.25)}, \quad (5)$$

for $\eta = 1.1 \times 10^{-3}$

$$r = 0.75 \sqrt{(z + 0.0289564)(0.367 - z)}. \quad (6)$$

Here z is the coordinate along the axis joining the pulsar and the star (it is assumed that the pulsar is located at the point “0”, and the optical star is located at $(z = -1, r = 0)$),

and r is the corresponding cylindrical radius (both coordinates are measured in the pulsar-star separation units, d_{p-s}). Eq.(6) shows non-smooth behavior at $z \simeq 0.367$. It does not have a physical meaning, but is the result of the simplification of the procedure which neglects the complex structure of the termination shock wave close to the symmetry axis (see Bogovalov et al. 2008, for details).

Since the particles in the pulsar wind move radially, the emission towards the observer is produced by electrons which were moving in this direction initially. The expected gamma ray flux is calculated as

$$\frac{dN}{dE_\gamma dS dt} = \frac{c}{4\pi d^2} \int_{\text{pulsar}}^{\text{termination shock}} dl \int d\epsilon_{\text{ph}} \int dE_e (1 - \cos\theta) e^{-\tau} \frac{d\sigma}{dE_\gamma} \frac{dN_e}{dE_e dl} \frac{dN_{\text{ph}}}{d\epsilon_{\text{ph}} dV}. \quad (7)$$

Here d is the distance to the system; $d\sigma/dE_\gamma$ is the differential anisotropic inverse Compton cross-section (Aharonian & Atoyan 1981; Bogovalov & Aharonian 2000); τ is the energy dependent optical depth due to gamma-gamma attenuation from the gamma ray creation point to the observer; and $dN_{\text{ph}}/d\epsilon_{\text{ph}}dV$ is the target photon density at the given location. The term representing the electron density in the cold pulsar wind has the following form:

$$\frac{dN_e}{dE_e dl} = \frac{L_{\text{sd}}}{\Gamma_0 mc^3} \delta \left(E_e - \Gamma_0 mc^2 - \int_0^l dl' \dot{E}/c \right), \quad (8)$$

where Γ_0 and \dot{E} are the initial wind bulk Lorentz factor and the electron energy loss rate.

The integration of Eq.(7) is performed over the line of sight from the pulsar location to the pulsar wind termination shock. Obviously, the integration path depends strongly on the orbital phase. In Figure 1, the lines of sight for three different orbital phases (-6 , 0 and 6 day from periastron passage) are shown by dashed lines.

Another effect, which may lead to an additional orbital phase dependence, is the shape of the optical star and temperature change between different regions of the star. To study this effect we performed calculation for the precise properties of the star, i.e. assuming the star to be an oblate spheroid with a linear gradient of the surface temperature as a function of the zenith angle. The orientation of the star in respect to the observer is defined by inclination angle, i.e. angle between the star rotation axis and line-of-sight, which was assumed to be $i_* = 33^\circ$, as inferred by Negueruela et al. (2011). To fix the star orientation an additional angle is required, namely the angle which describes the turn in the plane of the sky. This angle was assumed to be a free parameter, and its influence was studied. Numerical calculations show (see Figures 2 and 3) that independently on this parameter, the emission is well described by a model with a spherical star of radius $R_* = 6.2 \times 10^{11}$ cm

and surface temperature $T_* = 3 \times 10^4 \text{K}$. Given the uncertainties related to the orientation of the star, in what follows we perform calculations for the spherical star with the inferred parameters.

In Figure 2 we show the spectral energy distributions (SEDs) expected at the orbital phase corresponding to the periastron passage for $\eta = 1$ (solid lines); $\eta = 0.05$ (dotted lines); $\eta = 1.1 \times 10^{-3}$ (dashed line). In calculations we have adapted the following values of the initial wind Lorentz factors: $\Gamma_0 = 10^4, 4.6 \times 10^4, 2.2 \times 10^5$ and 10^6 . In Figure 3 we show a similar plot, but for the orbital phase corresponding to the epoch of 30 days before the periastron passage. For a rather broad range of the wind bulk Lorentz factors around $\Gamma_0 = 10^4$, the obtained flux level is above the *Fermi* sensitivity level (unless the η -parameter is small $\eta \ll 0.05$).

Due to the orbital phase dependence of several key parameters, in particular, separation distance, the location of the termination shock, the gamma-gamma optical depth, and the electron – target photon interaction angle, the pulsar wind signal has an orbital phase-dependence. Since the lightcurves for different energies are quite similar, we show just a few examples. In particular, the lightcurve for 10 GeV gamma rays is shown in Figure 4. Here we assumed for the initial pulsar wind Lorentz factor $\Gamma_0 = 4.6 \times 10^4$. In calculations we used two different values of the η -parameter: $\eta = 1$ (solid line) and $\eta = 0.05$ (dotted line). We note that this parameter may affect not only the flux level, but also the location of the light-curve maximum: in the case of the small value the maximum is located close to the periastron passage, while in the case of larger values of η the maximum is located a few days before periastron passage.

In the case of large bulk Lorentz factor, $\Gamma_0 \sim 10^{6-7}$, the inverse Compton (IC) signal from the pulsar wind may appear at energies beyond the range of *Fermi*/LAT. In this energy band, the atmospheric Cherenkov telescope arrays are more appropriate tools for probing the wind’s Lorentz factor (note that for this specific source, currently only the HESS array is able to monitor PSR B1259–63). In Figure 4 we show a light curve of 0.4 TeV gamma rays calculated for the η -parameter $\eta = 1$ and for the bulk Lorentz factor of $\Gamma_0 = 10^6$.

3. Impact of the higher luminosity of the optical star

In addition to gamma-radiation of the unshocked pulsar wind, we expect gamma rays (at higher energies) from the Compton scattering of shock-accelerated electrons (Kennel & Coroniti 1984). If the optical radiation density exceeds the density of the magnetic field, the IC gamma ray production proceeds in the saturation regime, thus the increased luminosity of the optical

star does not lead to amplification of the VHE gamma ray signal. On the other hand, for the recently reported luminosity of the optical star (Negueruela et al. 2011), the gamma-gamma opacity for VHE photons traveling from the pulsar to the observer, may be as large as 0.5, thus emission may be attenuated by a factor of 1.6. In Figure 5 we show the corresponding optical depth as a function of the phase for four different energies of gamma rays: $E_\gamma = 0.05, 0.15, 0.4, 1$ and 5 TeV. Note that the gamma ray absorption is strongest at the energy of 0.4 TeV, while at energies below 100 GeV and at multi-TeV energies it becomes negligible. We note however that the actual absorption level depends on the production region location, while the calculations in Figure 5 assume that the production occurs in the pulsar location. In particular, in Figure 4 two lightcurves for 0.4 TeV gamma rays are shown. The thick dash-dotted line corresponds to the flux level corrected for the gamma-gamma attenuation, while thin dash-dotted line shows the intrinsic flux level. It can be seen that the attenuation is somewhat weaker than it is expected from the opacity shown in Figure 5. The reason for that is rather simple, namely since the gamma ray production occurs along the line of sight in the pulsar wind zone (see Eq.(7)), some gamma ray photons suffer a weaker attenuation than the one shown in Figure 5.

Another important implication of the enhanced optical luminosity of the companion star for the production of VHE gamma rays is related to the so-called effect of Compton drag which leads to the reduction of the Lorentz factor of the wind before it terminates. Khangulyan et al. (2007) have argued that this effect could lead to a deficit of power available for acceleration of VHE particle at the termination shock. It has been shown, in particular, that if the optical star would have a luminosity close to $4 \times 10^{38} \text{erg s}^{-1}$, then the tendency of reduction of the TeV flux observed by HESS (Aharonian et al. 2005) close to the periastron passage may be explained by the reduction of the overall energy of the pulsar wind due to the Compton drag. The stellar luminosity reported by Negueruela et al. (2011) is remarkably close to the one speculated in Khangulyan et al. (2007), thus this effect now becomes more relevant to the observed TeV lightcurve. To describe the effect quantitatively, we have calculated the energy fraction lost by electrons emitted within the solid angle of π steradian towards the optical star. The result are shown in Figure 6 for different values of the initial wind Lorentz factor: $\Gamma_0 = 10^4$ (dash-dotted line), 4.6×10^4 (solid line), 2.2×10^5 (dashed line) and 10^6 (dotted lines). The η -parameter was assumed to be $\eta = 1$. The calculations show that this effect may lead to a significant decrease of the pulsar wind energy transported to the termination shock in the case of high values of the η -parameter, i.e. $\eta \geq 0.1$. This should lead to a proportional decrease of the VHE gamma ray production. Obviously, the Compton drag can be important only if the GeV flux from the pulsar wind is high. This radiation should be clearly detected by *Fermi*/LAT, unless the pulsar wind is strongly anisotropic. The detection of the pulsar wind signal with *Fermi* could allow a quantitative estimate of

the expected decrease of the VHE gamma ray production.

The Compton drag should lead as well to a decrease of the pulsar wind ram pressure in the collision region. However, given a relatively weak dependence of the termination shock shape on the η -parameter, it is unlikely that the Compton drag would change significantly the pulsar – optical star interaction regime.

4. Conclusion

Motivated by the recent revision of optical properties of LS 2883, the companion star of PSR B1259–63 (Negueruela et al. 2011), we present new calculations of high energy gamma ray fluxes using a realistic termination shock geometry as described in Bogovalov et al. (2008). Calculations show that the higher optical star luminosity is compensated, to a large extent, by the new estimate of the distance to the source. Thus, the new calculations of gamma ray fluxes are quite close to previous predictions based on the old gamma ray parameters of the optical star (see in Khangulyan et al. 2007). According to Figure 2, the 0.1–10 GeV gamma ray fluxes calculated for epochs close to the periastron passage are below the current upper limits obtained with EGRET (Tavani et al. 1996), and above the minimum fluxes detectable by *Fermi*/LAT for observation time of about 1 month. The pulsar wind radiation component can be identified by its distinct spectral shape. Another important feature of this emission is the expected modulation with the pulsar period on the top of the smooth orbital phase dependence. Indeed, since the emitting electrons move towards the observer almost with the speed of light, the gamma ray signal should have the second modulation reflecting the time structure of the striped pulsar wind. Although, a detailed shape of the fine lightcurve can be hardly obtained given a lack of any consistent description of the striped pulsar wind, a detailed search for this effect looks quite important for a consistent interpretation of the results obtained with *Fermi*/LAT Tam et al. (2011); Abdo et al. (2011).

The most important implication of detection of this component of gamma radiation would be the unique opportunity to measure the Lorentz factor of the pulsar wind. On the other hand, in the case of failure of detection of this component at GeV and/or TeV energies, the conclusions could be equally interesting and important. The possible reasons of non-detection of gamma rays from the unshocked wind could be: (i) an extremely powerful stellar wind, i.e. very low values of the η parameter; (ii) unconventional, i.e. very low ($\Gamma_0 \ll 10^4$) or very large ($\Gamma_0 \geq 10^6$) values of the pulsar wind bulk Lorentz factor. The first condition requires the pulsar to interact with the stellar disc all over the orbit. This implies a very specific realization in the sense of orientation of the stellar disc (namely the orbital plane

and the disc plane should almost coincide), which contradicts to the current expectations (Melatos et al. 1995; Bogomazov 2005; Bogovalov et al. 2008; Kerschhaggl 2010). However, we should note that one cannot exclude that the pulsar wind is strongly anisotropic. If so, the gamma ray signal should be anisotropic as well. This can be another reason for reduction of the gamma ray flux, which unfortunately would make the conclusions concerning the range of parameters Γ_0 and η less robust. Finally, one should mention that if the pulsar wind is not absolutely cold, electrons in the frame of the wind might have a rather broader distribution. This would make the gamma ray spectrum less distinct and smoother compared to the ones shown in Figures 2 and 3.

Regarding VHE energy gamma rays produced after termination of the wind, the new optical observations of Negueruela et al. (2011) imply a significant reduction of the flux of IC gamma rays produced by shock-accelerated electrons. All three main factors related to (1) the larger distance to the source, (2) the gamma-gamma attenuation, and (3) the Compton drag of the pulsar wind work in the same (negative) direction reducing the gamma ray flux by a factor of up to 10. Given that the previous studies based on the old optical observations already have required a significant fraction of the spin-down luminosity (5%–10%) to be released in TeV gamma rays, the revised energy requirements become almost unbearable. A possible solution to the energy budget crisis could be the Doppler boosting of radiation as suggested in Khangulyan et al. (2008). This important issues will be discussed elsewhere.

The work of S.V.Bogovalov have been supported by the Federal Targeted Program "The Scientific and Pedagogical Personnel of the Innovative Russia" in 2009-2013 (the state contract N 536 on May 17, 2010). M.R. acknowledges support by the Spanish Ministerio de Ciencia e Innovación (MICINN) under grant FPA2010-22056-C06-02, as well as financial support from MICINN and European Social Funds through a *Ramón y Cajal* fellowship.

REFERENCES

- Abdo, A. A., Fermi LAT Collaboration, Chernyakova, M., Neronov, A., Roberts, M., & Fermi Pulsar Timing Consortium, t. 2011, arXiv:1103.4108
- Aharonian, F. A., & Atoyan, A. M. 1981, *Ap&SS*, 79, 321
- Aharonian, F., et al. (HESS collaboration) 2005, *A&A*, 442, 1
- Aharonian, F., et al. (HESS collaboration) 2009, *A&A*, 507, 389
- Ball, L., & Kirk, J. G. 2000, *Astropart. Phys.*, 12, 335

- Ball, L., & Dodd, J. 2001, PASA, 18, 98
- Bogomazov, A. I. 2005, Astronomy Reports, 49, 709
- Bogovalov, S. V., & Aharonian, F. A. 2000, MNRAS, 313, 504
- Bogovalov, S. V., & Khangulyan, D. V. 2002, Astronomy Letters, 28, 373
- Bogovalov, S. V., Khangulyan, D. V., Koldoba, A. V., Ustyugova, G. V., & Aharonian, F. A. 2008, MNRAS, 387, 63
- Casares, J., Ribas, I., Paredes, J. M., Martí, J., & Allende Prieto, C. 2005, MNRAS, 360, 1105
- Casares, J., Ribó, M., Ribas, I., Paredes, J. M., Martí, J., & Herrero, A. 2005, MNRAS, 364, 899
- Chernyakova, M., Neronov, A., Aharonian, F., Uchiyama, Y., & Takahashi, T. 2009, MNRAS, 387, 63
- Casares, J., Ribó, M., Ribas, I., Paredes, J. M., Martí, J., & Herrero, A. 2005, MNRAS, 364, 899
- Grove, J. E., Tavani, M., Purcell, W. R., Johnson, W. N., Kurfess, J. D., Strickman, M. S., & Arons, J. 1995, ApJ, 447, L113
- Johnston, S., Manchester, R. N., Lyne, A. G., Bailes, M., Kaspi, V. M., Qiao, G., & D’Amico, N. 1992, ApJ, 387, L37
- Johnston, S., Manchester, R. N., Lyne, A. G., Nicastro, L., & Spyromilio, J. 1994, MNRAS, 268, 430
- Johnston, S., Ball, L., Wang, N., & Manchester, R. N. 2005, MNRAS, 358, 1069
- Kawachi, A., et al. 2004, ApJ, 607, 949
- Kennel, C. F., & Coroniti, F. V. 1984, ApJ, 283, 710
- Kerschhaggl, M. 2011, A&A, 525, A80
- Khangulyan, D., Hnatic, S., Aharonian, F., & Bogovalov, S. 2007, MNRAS, 380, 320
- Khangulyan, D. V., Aharonian, F. A., Bogovalov, S. V., Koldoba, A. V., & Ustyugova, G. V. 2008, International Journal of Modern Physics D, 17, 1909

- Kirk, J. G., Ball, L., & Skjaeraasen, O. 1999, *Astropart. Phys.*, 10, 31
- Melatos, A., Johnston, S., & Melrose, D. B. 1995, *MNRAS*, 275, 381
- McCollum, B. 1993, *BAAS*, 25, 1321
- Negueruela, I., Ribó, M., Herrero, A., Lorenzo, J., Khangulyan, D., Aharonian, F.A., *ApJL*
in press (arXiv:1103.4636v1)
- Neronov, A., & Chernyakova, M. 2007, *Ap&SS*, 309, 253
- Owocki, S. P., & Cohen, D. H. 2006, *ApJ*, 648, 565
- Sarty, G. E., et al. 2011, *MNRAS*, 411, 1293
- Tam, P. H. T., Huang, R. H. H., Takata, J., Hui, C. Y., Kong, A. K. H., & Cheng, K. S.
2011, arXiv:1103.3129
- Tavani, M., Grove, J. E., Purcell, W., et al. 1996, *A&AS*, 120, 221
- Tavani, M., & Arons, J. 1997, *ApJ*, 477, 439
- Uchiyama, Y., Tanaka, T., Takahashi, T., Mori, K., & Nakazawa, K. 2009, *ApJ*, 698, 911
- Vink, J. S., de Koter, A., & Lamers, H. J. G. L. M. 2000, *A&A*, 362, 295

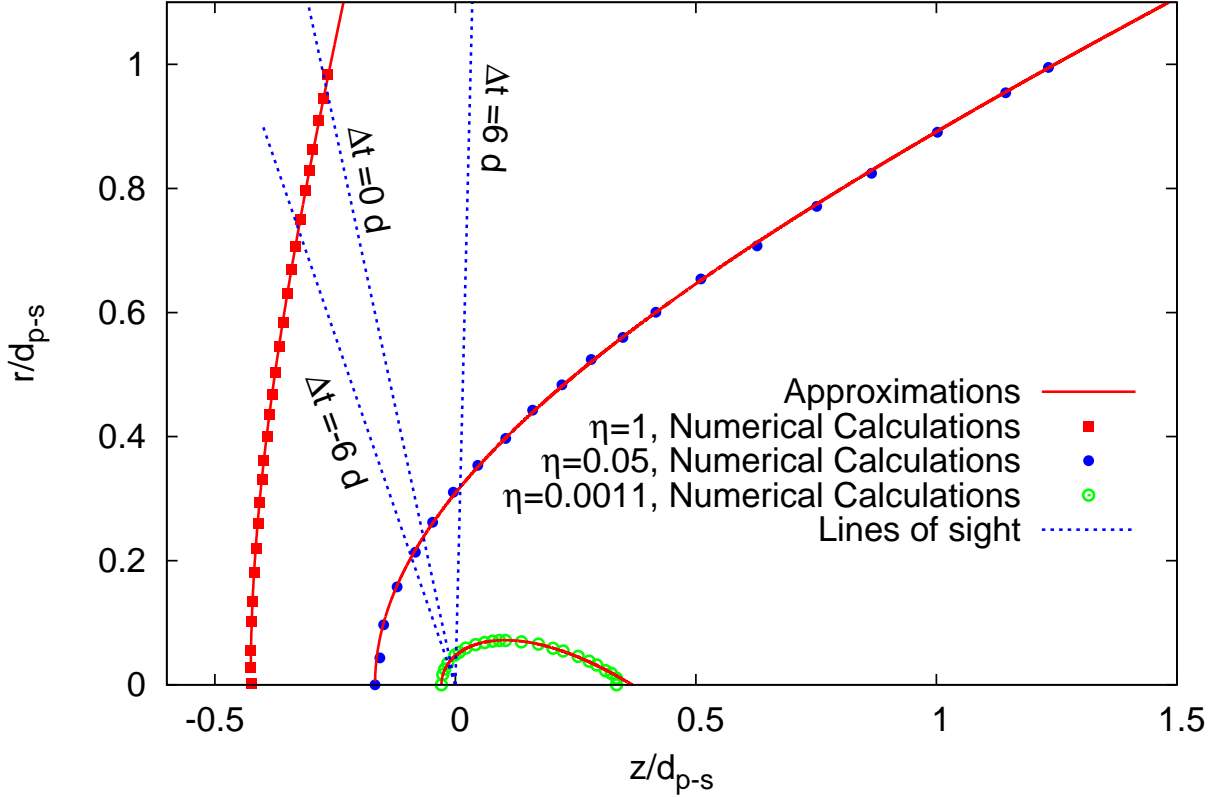


Fig. 1.— The geometry of interaction of pulsar and optical star winds: the pulsar is assumed to be located at the point with coordinates $r = 0$, $z = 0$, the optical star at $r = 0$, $z/d_{p-s} = -1$. The shapes of the termination shocks as obtained through the numerical modeling (Bogovalov et al. 2008) are shown for the following values of the η -parameter: $\eta = 1$ (squares), $\eta = 0.05$ (filled circles) and $\eta = 1.1 \times 10^{-3}$ (open circles). The analytical approximations Eq.(4-6) are shown with solid lines. The directions towards the observer are shown with dotted lines for three different epochs: -6 , 0 and 6 days to periastron passage.

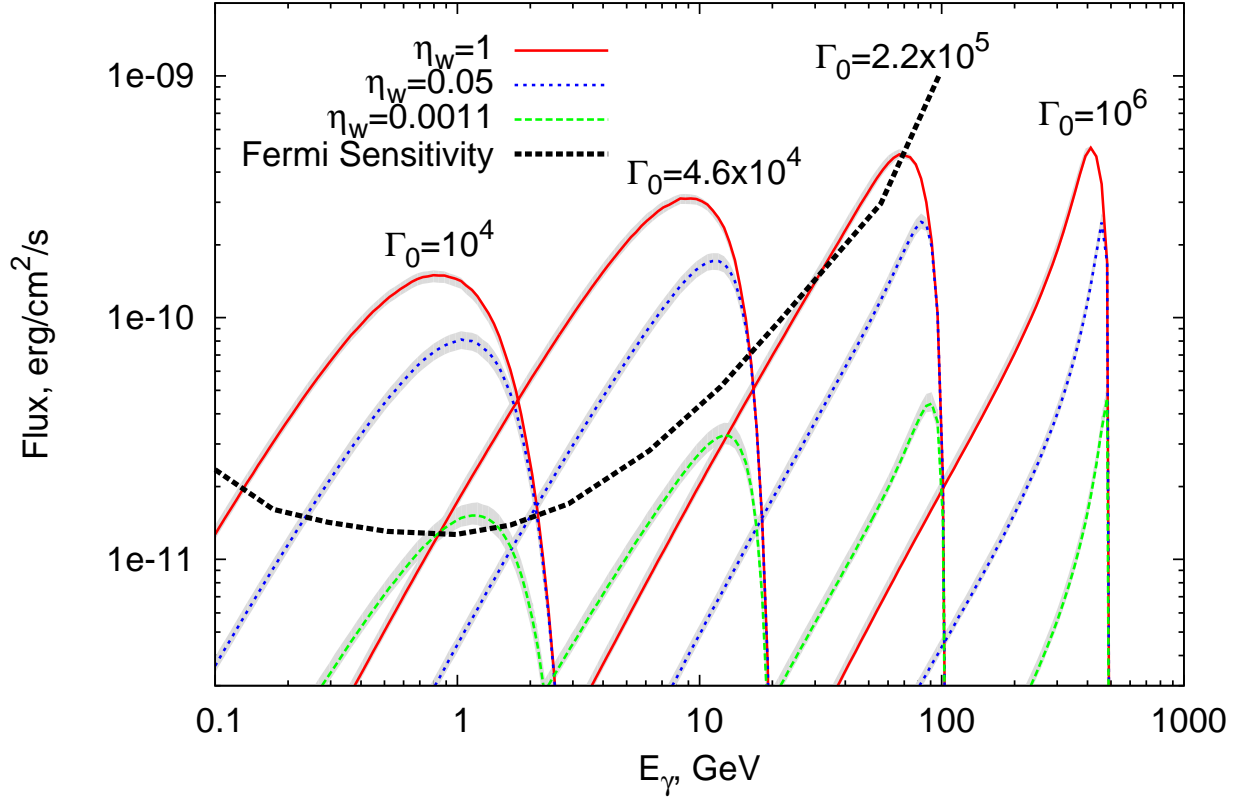


Fig. 2.— Spectral energy distributions of IC radiation from the unshocked pulsar wind for the epoch of periastron passage. The calculations were performed for different values of the η -parameter: $\eta = 1$ (solid lines), $\eta = 0.05$ (dotted lines) and $\eta = 1.1 \times 10^{-3}$ (dashed lines). The initial pulsar wind bulk Lorentz factor was assumed to be $\Gamma_0 = 10^4$, 4.6×10^4 , 2.2×10^5 and 10^6 . The thick dashed line roughly corresponds to the expected *Fermi* sensitivity for 0.1yr observation. The lines show model calculations performed for a spherical star with radius $R_* = 6.2 \times 10^{11}$ cm and surface temperature $T_* = 3 \times 10^4$ K; the regions filled with gray correspond to calculations with oblate star for possible star orientations.

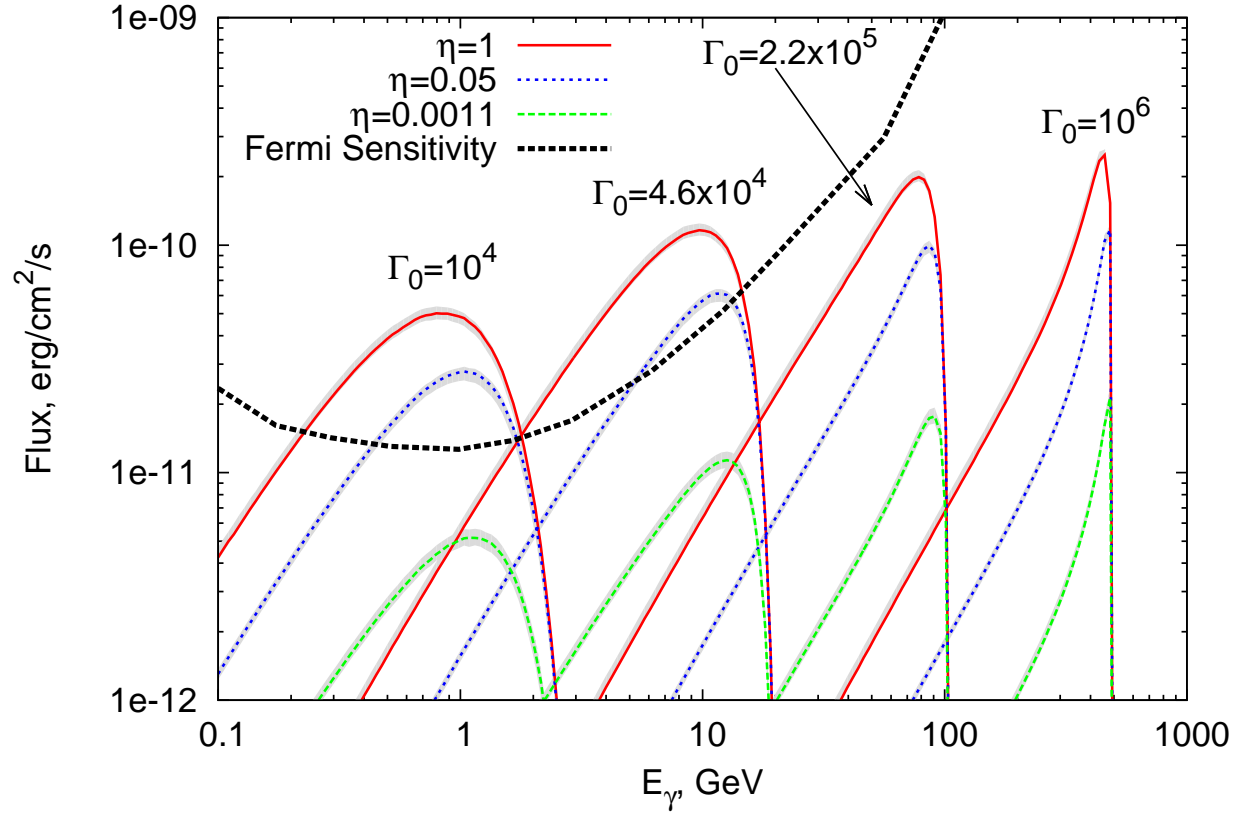


Fig. 3.— The same as in Fig.2 but for the epoch of 30 days before periastron passage.

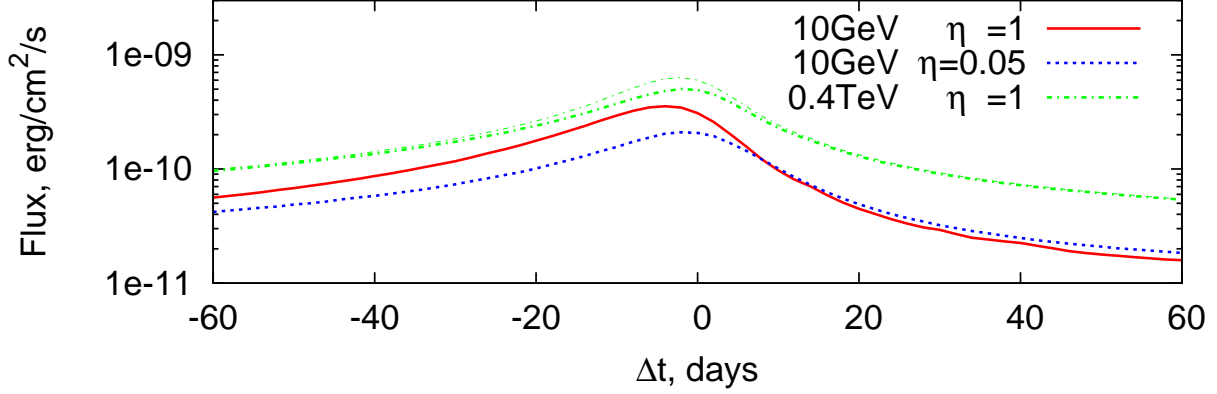


Fig. 4.— The solid and dotted lines show light-curves of 10GeV emission for two different values of the η -parameter: $\eta = 1$ (solid lines), $\eta = 0.05$ (dotted lines) for the initial pulsar wind bulk Lorentz factor of $\Gamma_0 = 4.6 \times 10^4$. Light curve of 0.4TeV gamma rays, calculated for $\eta = 1$ and the initial bulk Lorentz factor of $\Gamma_0 = 10^6$, is shown with thick dash-dotted line (accounting for gamma-gamma absorption) and with thin dash-dotted line without gamma-gamma attenuation. The calculations are performed for a spherical star with radius $R_* = 6.2 \times 10^{11}$ cm and surface temperature $T_* = 3 \times 10^4$ K.

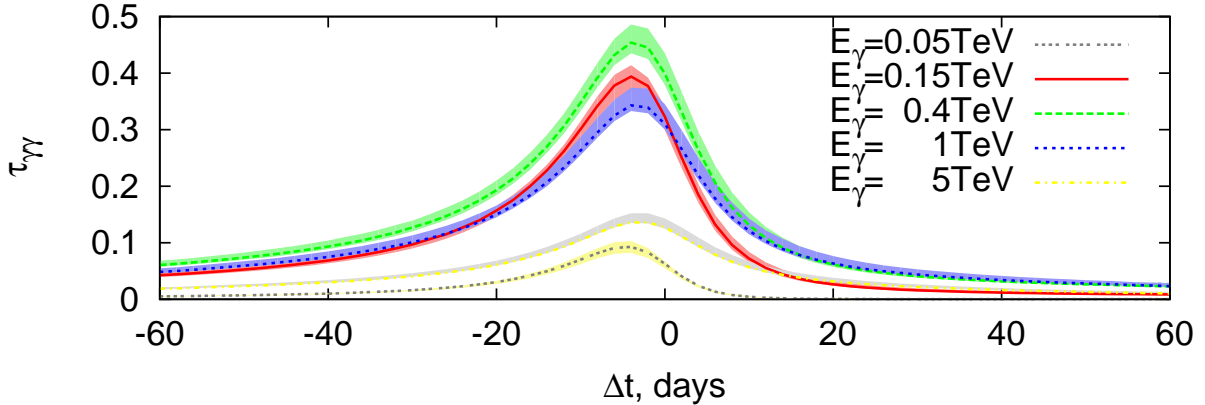


Fig. 5.— The optical depth for gamma-gamma attenuation from the location of the pulsar to the observer for different energies of the gamma rays. The lines show model calculations performed for a spherical star with radius $R_* = 6.2 \times 10^{11}$ cm and surface temperature $T_* = 3 \times 10^4$ K; the filled regions correspond to calculations with oblate star for possible star orientations.

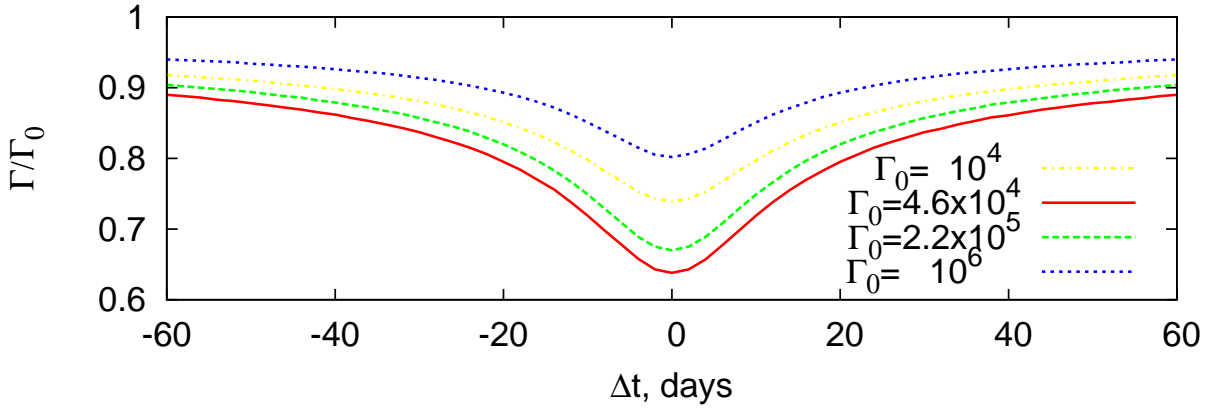


Fig. 6.— The averaged ratio of the electron Lorentz factor Γ at the termination shock to the initial value Γ_0 . The averaging is performed for electrons propagating within the angle of 60° towards the optical star. The ratio is calculated for the different values of the initial pulsar wind bulk Lorentz factor: $\Gamma_0 = 10^4$ (dash-dotted line), 4.6×10^4 (solid line), 2.2×10^5 (dashed line) and 10^6 (dotted line). The η -parameter was assumed to be $\eta = 1$, and the calculations are performed for a spherical star with radius $R_* = 6.2 \times 10^{11}$ cm and surface temperature $T_* = 3 \times 10^4$ K.